Optical near-field excitations on plasmonic nanoparticle-based structures

S. Foteinopoulou, J. P. Vigneron, and C. Vandenbem

Laboratoire de Physique du Solide (LPS), Facultés Universitaires Notre-Dame de la Paix (FUNDP), 61 rue de Bruxelles, B-5000 Namur, Belgium

sfoteino@iesl.forth.gr

Abstract: We investigate optical excitations on single silver nanospheres and nanosphere composites with the Finite Difference Time Domain (FDTD) method. Our objective is to achieve polarization control of the enhanced local field, pertinent to SERS applications. We employ dimer and quadrumer structures, which can display broadband and highly confined near-field-intensity enhancement comparable to or exceeding the resonant value of smaller sized isolated spheres. Our results demonstrate that the polarization of the enhanced field can be controlled by the orientation of the multimers in respect to the illumination, rather than the illumination itself. In particular, we report cases where the enhanced field shares the same polarization with the exciting field, and cases where it is predominantly perpendicular to the source field. We call the later phenomenon depolarized enhancement. Furthermore, we study a realizable nanolens based on a tapered self-similar silver nanosphere array. The time evolution of the fields in such structures show conversion of a diffraction limited Gaussian beam to a focused spot, through sequential coupling of the nano-array spheres' Mie-plasmons. For a longitudinally excited nanolens design we observed the formation of an isolated focus with size about one tenth the vacuum wavelength. We believe such nanolens will aid scanning near-field optical microscopy (SNOM) detection and the excitation of surface plasmon based guiding devices.

OCIS codes: (260.2110) Electromagnetic theory; (290.4020) Mie Theory (260.3910) Metals, optics of; (290.5850) Scattering, particles; (240.6680) Surface plasmons

References and links

1. R. Ruppin, "Spherical and cylindrical surface polaritons in solids," in *Electromagnetic Surface Modes*, pp. 345–398 (John Wiley & Sons, Belfast, 1982).
2. J. B. Jackson, S. L. Westcott, L. R. Hirsch, J. L. West and N. J. Halas, "Surface enhanced Raman effect via the nanoshell geometry," Appl. Phys. Lett. **82**, 257–259 (2003).
3. S. Schultz, D. R. Smith, J. J. Mock, and David A. Schultz,"Single-target molecule detection with nonbleaching multicolor immunolabels," Proc. Nat. Acad. Sci. **97**, 996-1001 (2000).
4. T. D. Corrigan, S. H. Guo, H. Szmacinski, and R. J. Phaneuf, "Systematic study of the size and spacing dependence of Ag nanoparticle enhanced fluorescence using electron-beam lithography," Appl. Phys. Lett. **88**, 101112 (2006).
5. K. Aslan, Z. Leonenko, J. R. Lakowicz, and C. D. Geddes, "Annealed silver-island films for applications in metal-enhanced fluorescence: Interpretation in terms of radiating plasmons," J. Fluoresc. **15**, 643–654 (2005).
6. S. A. Maier, P. G. Kik and H. A. Atwater, "Optical pulse propagation in metal nanoparticle chain waveguides," Phys. Rev. B **67**, 205402 (2003).

#75920 - $15.00 USD Received 9 October 2006; revised 19 February 2007; accepted 20 March 2007

7. M. Quinten, A. Leitner, J. R. Krenn, and F. R. Aussenegg, "Electromagnetic energy transport via linear chains of silver nanoparticles," Opt. Lett. **23**, 1331–1333 (1998).
8. C. Girard and R. Quidant, "Nearfield optical transmittance of metal particle chain waveguides," Opt. Express **12**, 6141–6146 (2004). http://www.opticsinfobase.org/abstract.cfm?URI=oe-12-25-6141.
9. T. Kalkbrenner, M. Ramstein, J. Mlynek, and V. Sandoghdar, "A single gold Particle as a probe for apertureless SNOM," J. Microsc. **202**, 72–76 (2001).
10. A. Alù, A. Salandrino, and N. Engheta, "Negative effective permeability and left-handed materials at optical frequencies," Opt. Express **14**, 1557–1567 (2006). http://www.opticsinfobase.org/abstract.cfm?URI=oe-14-4-1557.
11. A. N. Grigorenko, A. K. Geim, H. F. Gleeson, Y. Zhang, A. A. Firsov, I. Y. Khrushchev, and J. Petrovic, "Nanofabricated media with negative permeability at visible frequencies," Nature (London) **438**, 335–338 (2005).
12. A. Taflove and S. C. Hagness, *Computational Electrodynamics*, 2nd ed. (Artech House, Norwood, MA).
13. J.D. Joannopoulos, R.D. Meade and J.N. Winn, *Photonic Crystals, Molding the Flow of Light.* (Princeton Univ. Press, Princeton N. J., 1995).
14. S. Foteinopoulou, E. N. Economou, and C. M. Soukoulis, "Refraction in media with a negative refractive index," Phys. Rev. Lett. **90**, 107402 (2003).
15. C. Luo, S. G. Johnson, J. D. Joannopoulos, and J. B. Pendry, "All-angle negative refraction without negative effective index," Phys. Rev. B **65**, 201104 (2002).
16. R. W. Ziolkowski and E. Heyman, "Wave propagation in media having negative permittivity and permeability," Phys. Rev. E **64**, 056625 (2001).
17. C. Oubre and P. Nordlander, "Finite-difference time-domain studies of the optical properties of nanoshell dimers," J. Phys. Chem. B **109**, 10042–10051 (2005).
18. P. Nordlander, C. Oubre, E. Prodan, K. Li, and M. I. Stockman, "Plasmon hybridizaton in nanoparticle dimers," Nano Lett. **4**, 899–903 (2004).
19. P. B. Catrysse, H. Shin, and S. H. Fan, "Propagating modes in subwavelength cylindrical holes," J. Vac. Sci. Technol. B **23**, 2675–2678 (2005).
20. H. Shin and S. H. Fan, "All-angle negative refraction for surface plasmon waves using a metal-dielectric-metal structure," Phys. Rev. Lett. **96**, 073907 (2006).
21. P. G. Kik, S. A. Maier and H. A. Atwater, "Image resolution of surface-plasmon-mediated near-field focusing with planar metal films in three dimensions using finite-linewidth dipole sources," Phys. Rev. B **69**, 045418 (2004).
22. W. Challener, I. Sendur, and C. Peng, "Scattered field formulation of finite difference time domain for a focused light beam in dense media with lossy materials," Opt. Express **11**, 3160–3170 (2003). http://www.opticsinfobase.org/abstract.cfm?URI=oe-11-23-3160.
23. S. Foteinopoulou and C. M. Soukoulis, "Theoretical investigation of one-dimensional cavities in two-dimensional photonic crystals," IEEE J. Quantum Electron. **38**, 844–849 (2002).
24. G. Mie, "Beitrage zur optik trüber medien, spellzien kolloïdaler metallosungen," Ann. Physik **25**, 377 (1908).
25. M. Born and E. Wolf, *Principles of Optics*, 2nd ed. (Macmillan Co., New-York, 1964).
26. K. S. Kunz and R. J. Luebbers, *The Finite Difference Time Domain Method for Electromagnetics* (CRC Press, Boca Raton, FL, 1993).
27. J. L. Young and R. O. Nelson, "A summary and systematic analysis of FDTD algorithms for linearly dispersive media," IEEE Antennas Propag. Mag. **43**, 61–77 (2001).
28. S. A. Cummer, "An analysis of new and existing FDTD methods for isotropic cold plasma and a method for improving their accuracy," IEEE Trans. Antennas Propag. **45**, 392–400 (1997).
29. P. B. Johnson and R. W. Christy, "Optical Constants of the Noble Metals," Phys. Rev. B **6**, 4370–4379 (1972).
30. W. H. Press, B. P. Flannery, S. A. Teukolsky, and W. T. Vetterling, *Numerical Recipes* (Cambridge University, Cambridge, 1989).
31. P. G. Etchegoin, C. Galloway, and E. C. Le Ru, "Polarization-depedent effects in surface-enhanced Raman scattering (SERS)," Phys. Chem. Chem. Phys. **8**, 2624–2628 (2006).
32. J. Kottmann and O. Martin, "Plasmon resonant coupling in metallic nanowires," Opt. Express **8**, 655–663 (2001). http://www.opticsinfobase.org/abstract.cfm?URI=oe-8-12-655.
33. H. Xu, E. J. Bjerneld, M. Kall and L. Borjensson, "Spectroscopy of single hemoglobin molecules by surface enhanced Raman Scattering," Phs. Rev. Lett. **21**, 4357–4360 (1999).
34. J. P. Kottman and O.J.F. Martin, "Retardation-induced plasmon resonances in coupled nanoparticles," Opt. Lett. **26**, 1096 (2001).
35. E. Hao and G. C. Schatz, "Electromagnetic fields around silver nanoparticles and dimers," J. Chem. Phys. **120**, 357 (2004).
36. S. Enoch, R. Quidant and Goncal Badenes, "Optical sensing based on plasmon coupling in nanoparticle arrays," Opt. Express **12**, 3422–3427 (2004). http://www.opticsinfobase.org/abstract.cfm?URI=oe-12-15-3422.
37. I. Romero, J. Aizpurua, G. W. Bryant and F.J. Garcia de Abajo, "Plasmons in nearly touching metallic nanoparticles: singular response in the limit of touching dimers," Opt. Express **14**, 9988–9999 (2006). http://www.opticsinfobase.org/abstract.cfm?URI=oe-14-21-9988.

#75920 - $15.00 USD Received 9 October 2006; revised 19 February 2007; accepted 20 March 2007

38. R. Fuchs and F. Claro, "Multipolar response of small metallic spheres: Nonlocal Theory," Phys. Rev. B **35**, 3722 (1987).
39. J. Kottmann, O. Martin, D. Smith, and S. Schultz, "Spectral response of plasmon resonant nanoparticles with a non-regular shape," Opt. Express **6**, 213–219 (2000). http://www.opticsinfobase.org/abstract.cfm?URI=oe-6-11-213.
40. A. Karalis, E. Lidorikis, M. Ibanescu, J. D. Joannopoulos and M. Soljacic, "Surface-plasmon-assisted guiding of broadband slow and subwavelength light in air," Phys. Rev. Lett. **95**, 063901 (2005).
41. P. B. Catrysse, G. Veronis, H. Shin, J. T. Shen, S. Fan, "Guided modes supported by plasmonic films with a periodic arrangement of subwavelength slits," Appl. Phys. Lett. **88**, 031101 (2006).
42. R. Zia, M. D. Selker and M. L. Brongersma, "Leaky and bound modes of surface plasmon waveguides," Phys. Rev. B **71**, 165431 (2005).
43. K. Li, M. I. Stockman, and D. J. Bergman, "Self-similar chain of metal nanospheres as an efficient nanolens," Phys. Rev. Lett. **91**, 227402 (2003).
44. S. E. Sburlan, L. A. Blanco and M. Nieto-Vesperinas, "Plasmon excitation in sets of nanoscale cylinders and spheres," Phys. Rev. B **73**, 035403 (2006).
45. F. Dhili, R. Bachelot, A. Rumyantseva, G. Lerondel, and P. Royer , "Nanoparticle photosensitive polymers using local field enhancement at the end of apertureless SNOM tips," J. Microsc. **209**, 214–222 (2003).
46. A. Hohenau, H. Ditlbacher, B. Lamprecht, J. R. Krenn, A. Leitner and F. R. Aussenegg, "Electron beam lithography, a helpful tool for nanooptics," in press Micro. Eng.
47. R. Fikri, "Modelling of the apertureless near-field scanning optical microscope with the finite element method," Ph. D. thesis, Université de Technologie de Troyes (2003).
48. P. G. Kik, S. A. Maier, and H. A. Atwater, "Plasmon printing - a new approach to near-field lithography," Mat. Res. Soc. Symp. Proc. **705**, Y3.6 (2002).

1. Introduction

Metallic nanoparticles can mold and reshape the near field in a much more powerful manner compared to their dielectric counterparts. Significant enhancement of the electric field in the vicinity of the nanoparticle is therefore expected [1]. These characteristics have made such particles particularly appealing for many recent studies and related applications. For example, their near-field enhancing properties have been found to be of key importance in surface enhanced Raman spectra (SERS) [2]. Researchers have also utilized this property to suggest new means to label and identify biomolecules [3]. Silver nanoparticles can also enhance fluorescence spectra [4], in this way aiding in chemical sensing applications [5]. Many other studies have focused on the use of nanoparticle chains to achieve sub-diffraction electromagnetic transport [6, 7, 8]. Moreover, gold nanospheres have been added to apertureless Scanning-Near-Field-Optical-Microscope (SNOM) tips [9], to provide resolution controlled only by the particle-probe size and to reduce the effect of the background noise signal. More recently, it was found that nanoparticle-based structures can serve as building blocks of an artificial magnetic metamaterial [10, 11].

Undoubtedly, metal nanoparticles will play a leading role in the rapidly developing fields of nanoscience and technology. While, Mie theory describes efficiently the scattering of a plane wave source by a single metal sphere, it becomes highly complex and maybe inappropriate for large number of particles, for particles with non-spherical shape in arbitrary arrangement, and for realistic or multiple excitation sources. Consequently, it becomes important to be able to study electromagnetic excitations on metallic particles by means of a numerical method. The Finite Difference Time domain (FDTD) method [12] is a prominent technique in electromagnetics research and has led to the observation of many novel phenomena in resonator structures [12], photonic crystals [13, 14, 15] and negative index metamaterials [16]. Recently, this method has been also employed for the study of metallic nanostructures, such as silver nanoshells or nanoshell dimers [17, 18], plasmonic nanoguides [6, 19] and plasmonic superlenses [20, 21]. Challener et al. [22] investigated solid spherical silver particles with the FDTD technique and made a comparison with the respective Mie theory. Nevertheless, their study focused only on specific cases, involving either off-resonance near-fields or larger sub-micron

#75920 - $15.00 USD Received 9 October 2006; revised 19 February 2007; accepted 20 March 2007

sized particles. However, many of the aforementioned applications can benefit from the high-field values present in the vicinity of metallic nanosized particles, when excited on-resonance. Mie resonances for smaller sized metallic spheres typically have smaller linewidth and thus larger quality factors. This implies, that these cases would be comparatively intricate to model numerically [23]. Accordingly, it is rather important to briefly review the validity and limitations of the FDTD method for such cases by comparison with rigorous Mie calculations [1, 24, 25]. In this way, one can evaluate the applicability of this numerical approach to other more complicated nanoparticle-based structures.

We present an outline of the FDTD method used in all the simulations in Sec. 2. To ascertain the suitability of the FDTD method we model in Sec. 3 different silver spheres with radii ranging from 25nm-75nm, and compare the near field enhancement spectrum, and snapshots of the field distribution with Mie-theory calculations [25]. Subsequently, we explore the possibility to manipulate the polarization of the enhanced local field. We consider dimers and quadrumer structure under different illumination and orientations and present our results and conclusions in Sec. 4. Afterward, we research self-similar nanosphere arrays and find that these can convert a diffraction-limited Gaussian beam into a subwavelength focus with size $\sim \lambda_0/10$, with λ_0 being the vacuum wavelength. We demonstrate two different types of nanolens designs in Sec. 5. Lastly, we present our conclusions in Sec. 6.

2. The Finite difference time domain method in plasmonic structures

Typically, the FDTD technique relies on the solution of Maxwell's equation on a staggered grid lattice with leapfrog stepping in time (Yee algorithm [12, 26]). Although this method can incorporate trivially any dielectric medium, the same is not true for a dispersive material, because of the frequency dependence of the dielectric permittivity. Different schemes have been adopted thus far to handle dispersive materials in FDTD [12, 27]. We employ in this work the Auxiliary Differential Equation (ADE) method [12, 27, 28]. The later scheme dependents on the particular material dispersion relation, but is much more efficient in memory requirements in comparison with recursive convolution methods [27]. We use the Drude model, to represent the dispersive dielectric response , $\varepsilon(\omega)$, of the silver particles–i.e.,

$$\varepsilon(\omega) = \varepsilon_\infty - \frac{\omega_p^2}{\omega(\omega + i\Gamma_D)}. \tag{1}$$

The Drude model parameters in Eq. (1), namely the core dielectric constant, ε_∞, plasma frequency, ω_p, and the intrinsic damping parameter, Γ_D, are obtained by fitting on the Johnson and Christy [29] optical bulk experimental data for the frequency region of interest. Thus, we obtain $\varepsilon_\infty = 4.785$, $\omega_p = 14.385 \cdot 10^{15} rad/sec$, and $\Gamma_D = 7.95 \cdot 10^{13} rad/sec$.

The ADE method in dispersive media, relies on the Fourier transform of an associated polarization current,

$$\mathbf{J_P} = -j\omega\varepsilon_0\chi_e(\omega)\mathbf{E}(\omega), \tag{2}$$

with ε_0 being the vacuum permittivity, from frequency to time domain. In our case, $\chi_e(\omega)$ represents the electric susceptibility of the Drude medium. Then for propagation inside a Drude-material domain the relevant Eqs. are [27, 28]:

$$\partial_t \mathbf{E} = \frac{1}{\varepsilon_0\varepsilon_\infty}(\nabla \times \mathbf{H} - \mathbf{J_P}) \tag{3}$$

and

$$\partial_t \mathbf{J_P} + \Gamma_D \mathbf{J_P} = \varepsilon_0 \omega_p^2 \mathbf{E}. \tag{4}$$

#75920 - $15.00 USD Received 9 October 2006; revised 19 February 2007; accepted 20 March 2007

Equations (3) and (4) along with the third of Maxwell's equations (Ampere's law) are discretized on a three dimensional (3D) staggered grid lattice according to the Yee-algorithm. The resulting numerical scheme provides the evolution in space and time of the fields in the dispersive part of the computational domain. We alert the reader at this point regarding the sign convention in Eq. (2). It corresponds to fields varying in time with $\exp(-j\omega t)$, and requires a positive sign for Γ_D. All relevant signs should be modified accordingly, when fields vary in time as $\exp(j\omega t)$. We note, just like in FDTD modeling of dielectric structures, the computational domain is terminated with an absorbing boundary, to avoid any spurious back-reflections. In all the calculations that will be presented in the following, the silver nanoparticles are embedded in a glass matrix with refractive index, n, equal to 1.60. We therefore adopt a modified MUR absorbing boundary[12] based on an Enquist-Majda equation[12] for a phase velocity equal to c/n, – with c being the velocity of light.

3. FDTD modeling of single silver spheres: Comparison with Mie theory

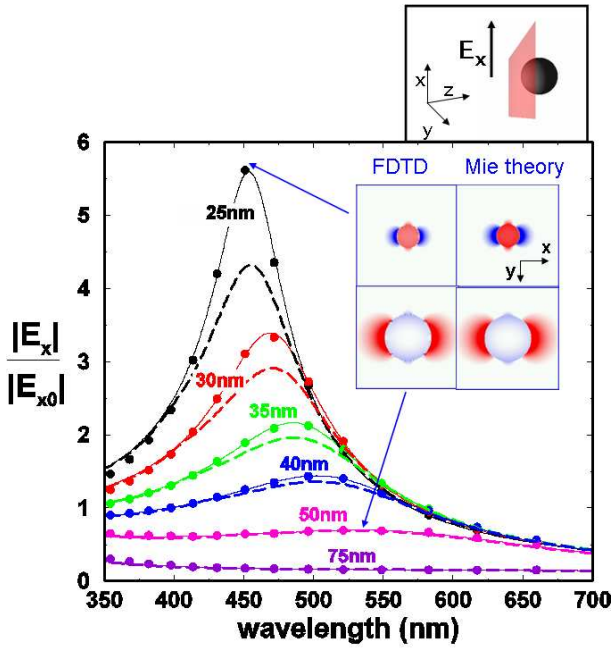

Fig. 1. Spectral response of the normalized near-field enhancement at the center of the nanoparticle. The plane of illumination and polarization of the source are shown in the upper panel. The dotted lines represent the FDTD results, while the solid lines the corresponding Mie calculations. The solid circles represent Mie calculations, where the actual tabulated Johnson and Christy data [29] are used for the dielectric function of silver. In the inset, we also show the on-resonance field distribution for two different nanoparticle sizes, –with radius 25 nm and 50 nm respectively– as indicated with the arrows.

We study the electromagnetic excitations on a single silver spherical particle with radius ranging from 25nm to 75nm, embedded in a glass medium. For this purpose, we perform FDTD simulations and will compare the results with corresponding Mie theory [25]. We adopt a cubic Yee cell with a side equal to 1 nm, and a time step dt=$1.54 \cdot 10^{-18}$ sec, bounded by the Courant condition [12, 27]. The particle is illuminated with a source with a Gaussian profile on the xy

#75920 - $15.00 USD Received 9 October 2006; revised 19 February 2007; accepted 20 March 2007

plane and electric field polarized along the x-direction, as indicated in the upper part of Fig. 1. A wide beam waist is chosen to emulate a plane wave propagating along the z-direction.

We concentrate on the near-field enhancement in the center of the nanoparticles. For this calculation we launch a pulsed signal in time, with central vacuum wavelength, λ_0= 476.2 nm and width, σ_t= 1.395 λ_0/c, in order to span the frequency area around the first Mie resonance of the silver nanospheres. Subsequently, we observe the evolution of the x-component of the electric field in the center of the particle, and apply a Fast Fourier Transform (FFT) [30] on the respective time series. This procedure yields the spectral dependence for the magnitude of the x-component of the electric field. The later quantity is normalized appropriately with the help of a second simulation run without the silver particle. We note at this point, it suffices to examine only the electric field parallel to the incident polarization, because at the center of the silver sphere the other electric field components are zero (or negligible in the FDTD). In this manner, we acquire the respective near-field enhancement at the silver sphere center, which is shown versus the free space wavelength with the dotted lines in Fig. 1. The solid lines represent the corresponding Mie calculations, when the Drude model [Eq. (1)] is used to describe the silver permittivity function. For comparison, we also show the expected Mie result of the enhancement when the actual values from the Johnson and Christy [29] tabulated data are used for the dielectric function of silver.

Figure 1 attests an excellent agreement for the resonant wavelength of the near-field enhancement spectrum between Mie theory and the FDTD. We also observe generally a very good agreement for the corresponding peak height. We notice, that the FDTD peak-heights are consistently a little lower than the respective Mie theory ones. This small difference, which is more pronounced for the smaller particles, is caused by the staircase that approximates the spherical surface of the nanoparticle in the Cartesian numerical grid. It is not surprising that this staircase effect is stronger for the smaller spheres. We see these are characterized by a relatively higher-quality-factor resonance, which would be more sensitive to structural and simulation parameters [23]. It is expected, that small imperfections in the surface of experimentally realizable nanoparticles could lead to a similar type of effect. For the same reason, for small to moderate particle sizes (radius ranging between 25 nm and 50 nm), frequencies approaching the second Mie resonance should be avoided. As these typically involve a large quality factor, they would pose much higher demands in spatial discretization and consequently in cpu memory requirements. Put it differently, the proper mesh size in FDTD modeling of metallic nanoparticles is dictated not only by the relevant frequency but also by the quality factor of their characteristic resonances.

We also compared the snapshots of the electric field, for the silver spheres of different sizes. These are sampled at a certain moment after steady state is reached. In each case the nanoparticle is excited with a quasi-monochromatic wave [14], with frequency set to be close to the respective Mie-resonance. We depict the x-component of the electric field, on the xy plane in the inset of Fig. 1, for two characteristic sphere sizes. The left panel displays the results from FDTD, while the right panel the results from Mie theory [25]. In order to make the comparison between FDTD and Mie theory, a phase factor multiplies the Mie calculated fields. In this way, the two fields (from FDTD and Mie theory) are compared at the same time instant of the full periodic cycle. We observe an excellent agreement in the electric field patterns, especially for the larger particle sizes.

Accordingly, we reviewed the parameters and restrictions for the reliable modeling of silver nanospheres by the FDTD technique. We will use these particles as the fundamental building blocks to construct composite structures which can exhibit new interesting phenomena, such as polarization selective enhancement and nano-lensing. Verification of this type of phenomena with an ab-initio method, like the FDTD, is of outmost important. Since the retardation effects

#75920 - $15.00 USD Received 9 October 2006; revised 19 February 2007; accepted 20 March 2007

of the EM field are taken into account, the calculated results provide solid grounds for the possibility of realization of the reported phenomena.

4. Field enhancement in multimer nanosphere-based configurations

In this section, we attempt to achieve an increased enhancement in the field intensity, with controlled polarization. We discussed earlier, that such enhancement is desirable for many near-field applications. One common route explored thus far, is to benefit from the field around small nano-sized metallic spheres when these are excited on resonance. As we also see in Fig. 1, this field becomes higher the smaller the particle. Nevertheless, this route toward high field enhancement entails some disadvantages. First, there is a limit of how small a nano-particle can be attained. Actually, the smaller the size the more challenging it becomes to fabricate a metallic nanosphere in a controlled and uniform manner. On top, as we also discussed in the previous section, surface roughness is expected to have a stronger impact on the overall enhanced local-field for the case of smaller nanospheres. Furthermore, enhancement based on single spheres, has mixed polarization. In fact, single spheres lead to an enhanced field, both along and perpedincularly to the exciting field. As a result, there is poor control over the polarization of the enhanced local field. The later is believed to be a factor seriously hindering the clear interpretation and reproducibility of SERS signals [31].

Therefore, we utilize multimers comprising of silver spheres with radius equal to 50 nm, and investigate whether such structures can produce an enhancement which is comparable to that of a smaller sphere with 25 nm radius. We note in passing, that other works have explored the possibility of achieving high enhancement with dimer configurations of nanorods [32, 34] or nanospheres [33, 35]. Nevertheless, polarization manipulation of the enhanced field is not discussed in any of the aforementioned works. In our subsequent study we explore the conditions of illumination, as well as the configuration and orientation of the silver sphere multimers that would lead to an enhancement with controlled polarization. We concentrate on the frequency range between 480nm and 1400nm, where Mie theory and FDTD show a very good agreement for the near field surrounding a 50 nm-radius silver sphere. In order to span this frequency region two different pulsed measurements,– centered at $\lambda_0 = 909.1$ nm, and $\lambda_0 = 588.3$ nm respectively–, are performed in the FDTD simulation. The spectra are always obtained with FFT [30], from the time sequence representing the evolution of the electric field at a certain detector point. We stress, that whenever we refer to near-field intensity enhancement in this section, we mean the intensity of the electric field normalized by its respective value in the absence of the metallic nanoparticles.

We first consider a dimer of touching silver spheres. This can be aligned in respect to the incident illumination in several ways. Let $\hat{d}$ represent the dimer axis, and xy the plane of illumination, with the incident source polarized along x. First we study a dimer with axis oriented along the incident field, i.e., along x. We consider detectors at 25 nm, 30 nm and 35 nm away from the touching dimers, along the z- and y-direction. We monitor the evolution of a pulsed signal in time, at these specified points shown in the upper panel of Fig. 2. Figure 2(a) displays the intensity enhancements for the detectors lying along the z-axis. Accordingly, Fig. 2(b) shows the intensity enhancements for detectors lying along the y-axis. The color of each curve matches the color of the detector which is pointed-out in the upper panel of the figure. We observe two peaks in each spectrum indicated with the bold arrows, around a free space wavelength, λ_0, equal to 625 nm and 1136 nm respectively. We found that the observed bi-resonant profile of the local field enhancement starts disappearing as the two spheres seize to touch and quickly vanishes with increasing separation. This behavior is consistent with previous observations on touching metallic disks [36] and was recently attributed to a different charge redistribution when the dimer spheres touch [37]. Alternatively, one could view the con-

#75920 - $15.00 USD Received 9 October 2006; revised 19 February 2007; accepted 20 March 2007

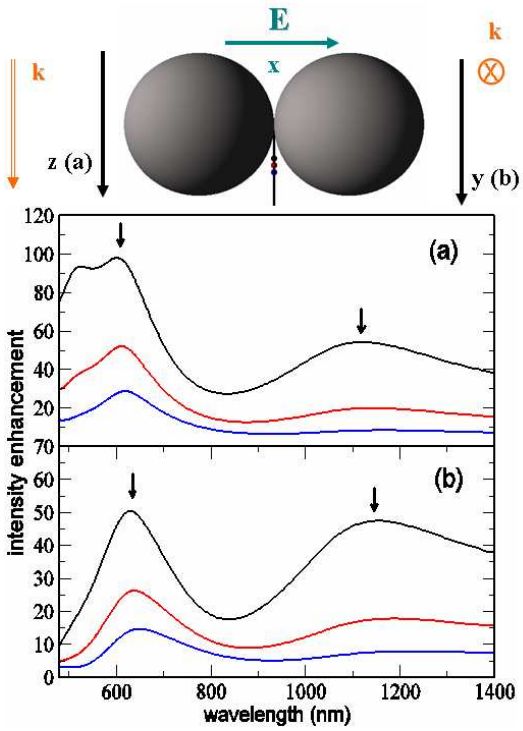

Fig. 2. Spectral response of the near field intensity enhancement in the vicinity of touching dimers. The top panel indicates the position of the detectors where the field is monitored. The vertical axis represents the z direction, i.e. the illumination direction for case (a) and the y-direction, i.e., the normal to both the illumination direction and exciting field polarization, for case (b). The color of the plotted lines matches the color of the specified detector.

tacting dimer as a system two distinct grooves which could exhibit multiresonant behavior in analogy with that observed in triangular particles [39]. We stress, that the dominant contribution to the field enhancement spectrum comes from the electric field component that is parallel to the incident field. We will see in the following that this is not always the case.

We also calculate the intensity enhancement in the entire 3D space for selected frequencies. For this purpose, we excite the touching dimer with a quasi-monochromatic Gaussian source at a certain free space wavelength, λ_0. The illumination conditions are otherwise the same as in Fig. 2. In each case, two simulations runs are necessary to obtain the intensity enhancement, I. Specifically,

$$I(x,y,z) = \frac{\frac{1}{2}\varepsilon_0\varepsilon_{glass}\sum_{t_0}^{t_0+T} E_x^2(x,y,z,t)+E_y^2(x,y,z,t)+E_z^2(x,y,z,t)}{\frac{1}{2}\varepsilon_0\varepsilon_{glass}\sum_{t_0}^{t_0+T} E_{0x}^2(x,y,z,t)+E_{0y}^2(x,y,z,t)+E_{0z}^2(x,y,z,t)}, \tag{5}$$

where, ε_0 is the vacuum permittivity and ε_{glass} is the relative permittivity of glass. The summation yielding the time-averaged value of the intensity starts at time t_0, after steady state is reached, and completes after an entire cycle of period, T. The denominator represents the time averaged intensity obtained in a run without the presence of the dimers,– needed for normalization. We illustrate the intensity enhancement distribution both on an xy plane cutting through the middle of the dimers (top panel of Fig. 3), and in the entire 3D space (middle

#75920 - $15.00 USD Received 9 October 2006; revised 19 February 2007; accepted 20 March 2007

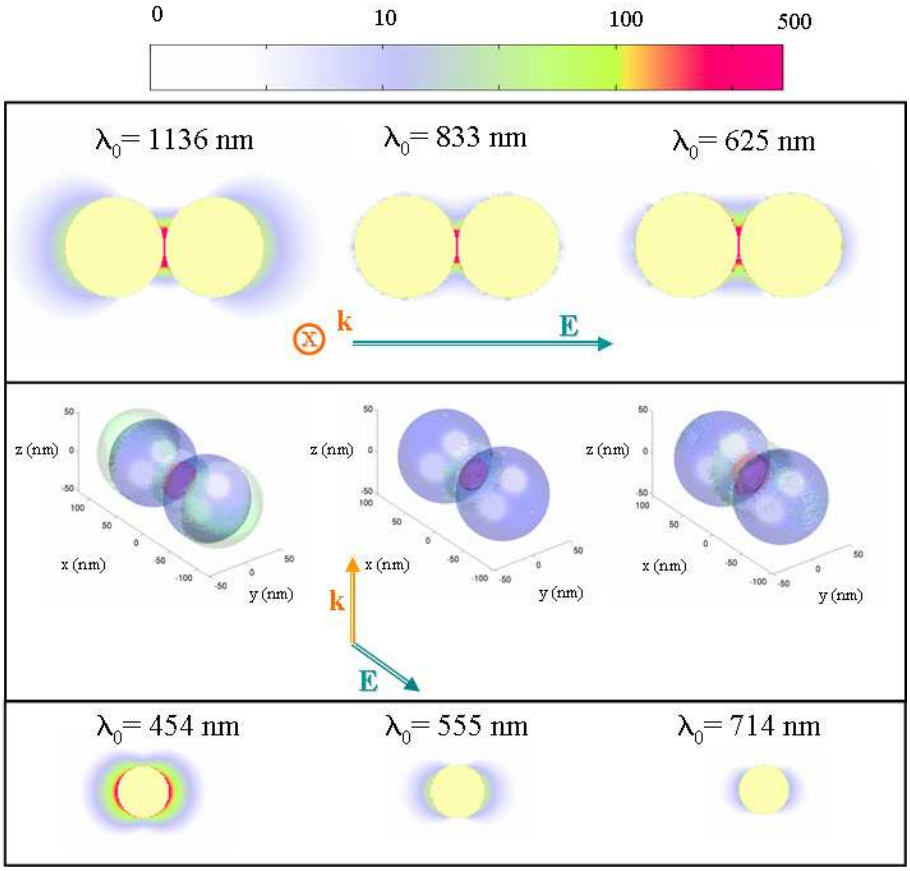

Fig. 3. Normalized time averaged intensity plots for three different excitation wavelengths: λ_0=1136 nm (left panel), 833 nm (middle panel) and 625 nm (right panel). In each case we see the intensity on the xy- plane slicing through the middle of the dimer, as well as in the entire 3D space. The 3D plots display two iso-intensity surfaces, representing an enhancement value of 100 (red) and 10 (green) respectively. For comparison in the bottom panel we show the intensity enhancement around a single silver sphere with 25 nm radius, on and off- resonance

panel of Fig. 3). The excitations wavelengths we have selected correspond to the two peaks of Fig. 2, – at 1136 nm and 625 nm respectively–, and the in-between valley, at 833 nm. The 3D plots depicted in the middle panel for the same wavelengths are iso-intensity plots. The green surfaces, enclose the space in the outer neighborhood of the dimers where the normalized intensity enhancement exceeds the value of 10. Conversely, the red surfaces enclose the space in the outer part of the dimers where the normalized intensity enhancement exceeds the value of 100. It is interesting to observe, that in all cases the interstitial region between the two spheres is characterized by a high enhancement factor. However, the area this enhancement covers is quite larger for the wavelengths corresponding to the peaks of the spectrum, and especially for case with $\lambda_0 = 1136$ nm. For comparison, we also plot the intensity enhancement for a silver nanosphere with 25 nm radius, as calculated from Mie theory, in the bottom panel of Fig. 3. The left-bottom graph represents an excitation on-resonance, while the other two adjacent

#75920 - $15.00 USD Received 9 October 2006; revised 19 February 2007; accepted 20 March 2007

graphs represent red-shifted excitation wavelengths away from the resonance. For the single 25nm-radius silver particle, we observe a significant enhancement only for the resonant wavelength. Even the later though, does not surpass the enhancement values we found in the dimers comprising of the larger spheres. Evidently, single particles exhibit rather a frequency selective enhancement while dimers produce a more broadband response.

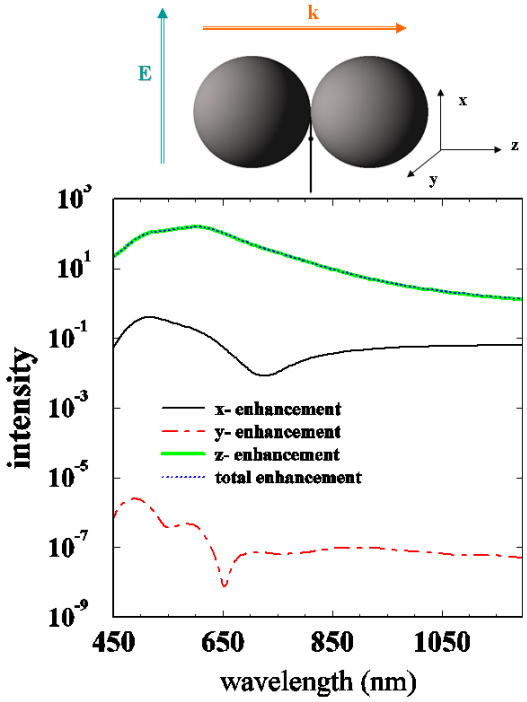

Fig. 4. Intensity enhancement for a dimer illuminated as shown in the upper schematics, at the indicated detector point. The contributions of the different components of the electric field to the total intensity enhancement are shown separately. It is clear, the predominant contribution comes from the field along the wave vector (orange vector), which is perpendicular to the illumination plane. In other words, the enhanced field became orthogonal to the driving field. Thus, we observed a depolarized enhancement phenomenon.

We flip now the dimer and orient it's axis along the y-direction, i.e. perpendicularly to both the polarization of the incident field and it's wave vector, **k**. In this configuration we did not observe any significant intensity enhancement. We rotate once more the dimer and make it parallel to the wave vector of the driving field, and witness a rather striking effect. While the electric field parallel to the exciting field is weak, the electric field along the illumination direction, z-, is very strong. In other words, the enhanced fields are "almost" completely depolarized in respect to the incident fields. This can be seen in Fig. 4, where we plot the spectral response of the different field components sampled at the point indicated in the upper panel. The solid black, dashed red, and solid green curves represent the contributions to the intensity enhancement corresponding to the x-, y- and z- component of the electric field respectively. In logarithmic scale we see that the contribution from the z- component of the electric field is almost two orders of magnitude more than the contribution from the x- component and more than seven orders of magnitude more than the contribution from the y-component.

#75920 - $15.00 USD Received 9 October 2006; revised 19 February 2007; accepted 20 March 2007

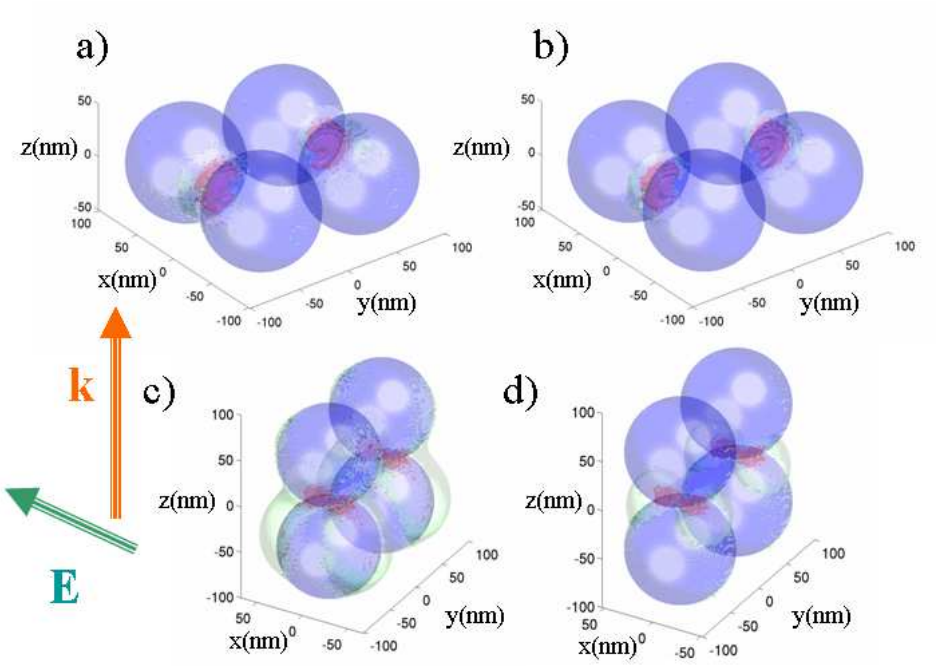

Fig. 5. Iso-surfaces representing an intensity enhancement value of 100 (red) and 10 (green) for quadrumers lying on the illuminating plane (top panel), or normally to the illuminating plane (bottom panel). We show the total enhancement [left: in (a) and (c)] and the enhancement corresponding to the major contributing field component, which is along x for case (b) and along z for case (d).

As dimers lead to a larger enhancement than the one stemming from the constituent spheres, it becomes an obvious choice to also explore configurations with more particles. For this reason, we considered touching quadrumers, for different orientations in respect to the illuminating field. We did not find an increased enhancement and overall their behavior is somewhat similar to that of the dimers. This is not surprising, as the high-field values seem confined in the two-sphere interstitial region. In other words, quadrumers act like two non-interacting dimers put together. It is not obvious to determine which are the parting dimers, as this depends on the particular illumination conditions. In the quadrumer structures we also found cases with polarized and depolarized enhancement. We show two such examples in Fig. 5. In the top panel the quadrumer lies on the plane of illumination (xy-plane). In the bottom panel the quadrumers lie on the yz plane and are thus perpendicular to the polarization of the incident source. To evaluate the quality of the polarized or depolarized enhancement we show the iso-intensity surfaces, both for the total intensity (left-panel) and only the contribution from the predominant field component (right-panel). The predominant field component is along the field of the incident source for the case of the quadrumers lying on the xy-plane, i.e. we have polarized enhancement. Conversely, the predominant field component is along the wave vector of the incident source for the case of the quadrumers lying on the yz-plane, i.e. we have depolarized enhancement. Notice the remarkable agreement between the predominant and total intensity enhancement for the case of polarized enhancement [Figs. 5 (a) and 5(b)]. For the yz-quadrumer configuration we find almost complete depolarization in the interstitial region, but we observe some enhancement in the outer sphere region coming from fields parallel to the incident source. The later intensities

#75920 - $15.00 USD Received 9 October 2006; revised 19 February 2007; accepted 20 March 2007

are though by far smaller than the values in the interstitial regions. This means that for practical purposes we can say that the enhancement is depolarized in such a case.

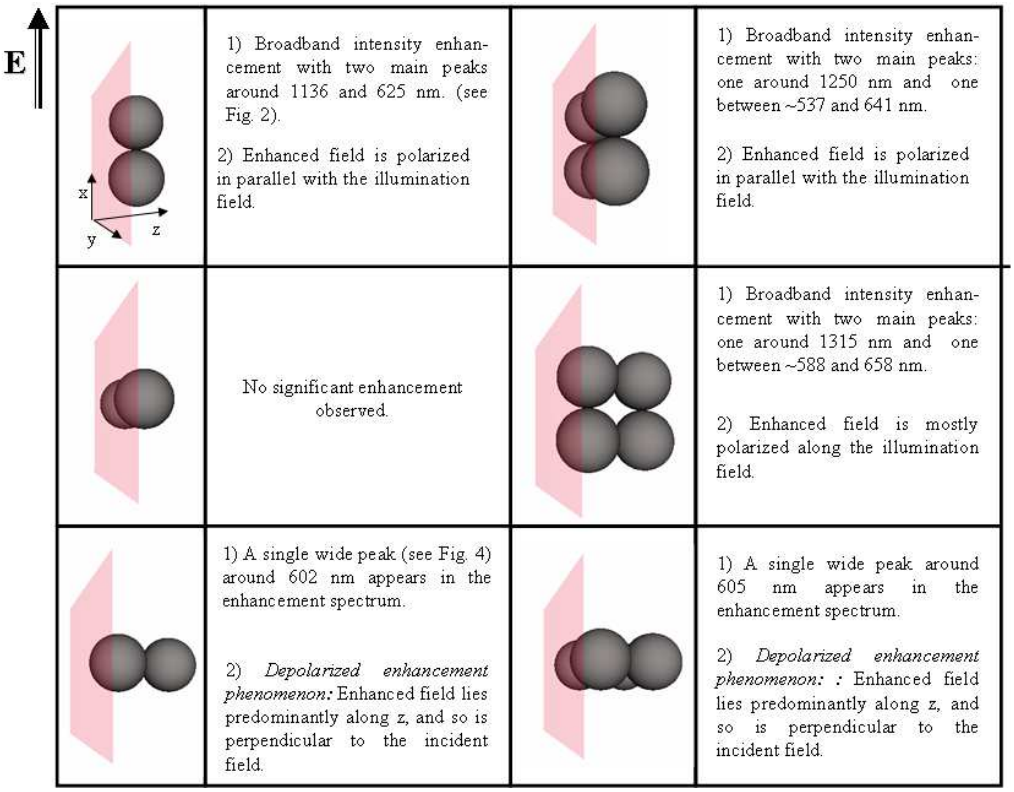

Fig. 6. Outline of different cases studied in this section. The spectral response as well as the type of enhancement, – polarized or depolarized–, is briefly described for each case.

We outline all cases that we studied for dimers and quadrumers in Fig. 6. We always kept the illuminating plane to be the xy plane, yielding a propagating wave with wave vector along z. The polarization of the incident source is along the x-axis. Then, the dimer and quadrumer structures are rotated in different ways, to encompass all possible relations between their orientation and illumination. The peaks of their spectral response are determined from several detectors placed in the vicinity of the contact points. From Fig. 6 we deduce that enhancement occurs when the nano-composite has a structural direction either along the incident field, or along the wave vector of the incident field. Hence, we observe field enhancement with quadrumers for any conditions, and no enhancement for dimers along the y-direction. We get depolarized enhancement if the nano-particle composite has no structural direction along the direction of the illuminating field. Otherwise, the enhancement is mostly highly polarized, especially if in addition the nano-composite does not also share a structural direction with the direction of the incident field wave vector. Moreover we found that a really broadband enhancement, – beginning from the near-infrared all the way to the visible–, occurs for the arrangements that have a structural direction along the driving electric field (**E**). To resume, we have found a way to predict and control the polarization of the enhanced local field, which can be a key factor for SERS based detection methods [31].

We note in passing, that non-local effects [38] have not been taken into account in the calcu-

#75920 - $15.00 USD Received 9 October 2006; revised 19 February 2007; accepted 20 March 2007

lations. The latter may impact the enhancement factors of the cases with a dimer or quadrumer axis along the incident field. However, we do not expect these would affect our conclusions regarding the polarization dependence of the local enhanced field, on the specific relations between structure orientation and illuminating field. Actually, we checked that these conclusions survive even for a small (2 nm) interparticle distance where it is known that non-local effects are really minor [35].

5. Nanoparticle based lens

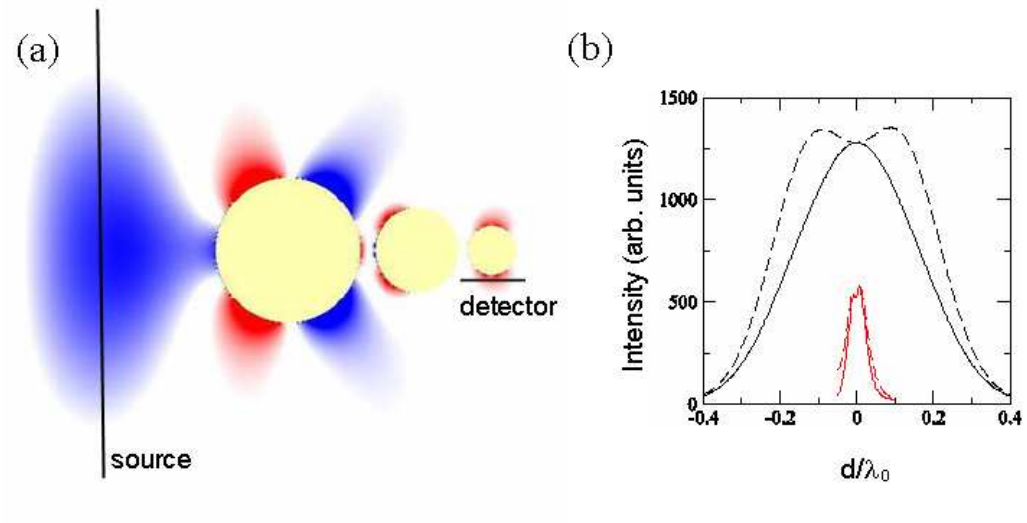

Fig. 7. (a). (1.55 MB) Self-similar silver nanosphere array acting as a nanolens. A Gaussian source polarized perpendicularly to the array axis is converted into foci with spot size about one tenth the vacuum wavelength, λ_0. (b) The time averaged intensity in source (black lines) and focus plane (red lines). The dotted lines represent the total intensity, while the solid lines represent the contribution from the component of the field parallel to the incident source polarization.

In the previous section we discussed how nanoparticles mold the near-field, to provide high electric field enhancement when interacting with each other. In this section we explore the possibility for nanoparticles to manipulate a relatively wide beam excitation into a narrow subwavelength focus. In fact, foci obtained with conventional optical instruments are bounded by the diffraction limit, which is roughly half the wavelength. However, with the advent of plasmonic devices [6, 40, 41, 42] subwavelength control of the excitation source becomes of outmost importance.

We follow upon the proposal of Li et al. [43] and consider a self-similar chain of silver particles, embedded in glass. The latter design was also studied under plane wave illumination by Sburlan et al. [44], for its near-field enhancement properties. The diameter and center-to-center distance corresponding to the first particle is taken 150 nm and 135 nm respectively. The ratio of self-similarity is taken equal to $1/\sqrt{3}$. We excite the chain with a Gaussian beam with a waist around $\lambda_0/2$, representing the diffraction limit. The electric field of the source is along the x-axis and so polarized perpendicularly to the axis of the chain (z-axis). We show a snapshot of the x-component of the electric field on the xz plane after steady state is reached in Fig. 7(a). The excitation wavelength, λ_0, is 500 nm. The corresponding movie, shows how the initial beam

#75920 - $15.00 USD Received 9 October 2006; revised 19 February 2007; accepted 20 March 2007

induces a Mie-plasmon in the first particle that sequentially couples from one sphere to the next in the self-similar chain. In this manner the incident diffraction limited beam is converted into small focused spots with size of the order of one tenth the free space wavelength, λ_0. In order to evaluate the performance of the conversion we plot the intensity along the source and focus plane in Fig. 7(b). We show the intensities corresponding to the x-component of the electric field (solid lines), as well as the total electric field intensities (dotted lines). The black lines correspond to intensities at the source plane while the red lines at the image plane. The focus above the last particle is symmetric to the focus below, therefore we show only the intensity for the later. The results in Fig. 7(b) manifest that the foci are highly polarized along the incident source, and each have intensity about 50% the incident source value. We also tested this nanolens design at other frequencies. We found however either an absent focus, or a spatial overlap between the Mie-plasmons of the second and last nanoparticles. For excitation at 833 nm we observed a strong background signal, quite possibly steming from the direct interaction of the source with the last particle. So, the optimum behavior is obtained at frequencies close to the Mie resonance of the middle nanoparticle, which is the case of Fig. 7.

Indeed, the self-similar nanosphere array of Fig. 7 does exhibit an interesting conversion of a diffraction limited Gaussian beam into two subwavelength foci, thus acting as a nanolens. We attribute this effect to a near-field interaction between the Mie plasmons of the individual particles. Despite the interesting nature of this phenomenon, there is a certain disadvantage to this design. Due to the location of the foci in the array, it is rather hard to use them subsequently to excite a plasmonic device [6, 40, 41, 42] or as a source for subwavelength lithographic patterning [45]. Therefore, in the following we investigate for an alternative nanolens design, which would lead to a subwavelength focus in a more functional location for these type of applications.

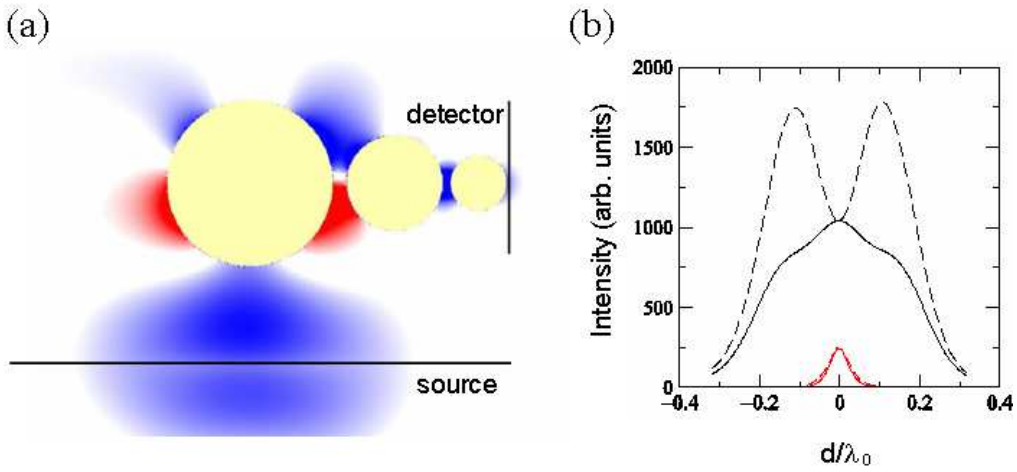

Fig. 8. (a). (2.064 MB) Another design of a self-similar-silver-nanosphere-array nanolens. A Gaussian source polarized parallelly to the array axis is converted into a subwavelength focus with size of the order of one tenth the vacuum wavelength, λ_0. (b) The time averaged intensity in source (black lines) and focus (red lines) plane are also shown. The dotted lines represent the total intensity, while the solid lines represent the contribution from the component of the field parallel to the incident source polarization.

We choose a diffraction limited Gaussian beam which illuminates the self-similar nanosphere

#75920 - $15.00 USD Received 9 October 2006; revised 19 February 2007; accepted 20 March 2007

array with electric field parallel to the array axis. The beam is targeted toward the first sphere of the chain. To avoid direct illumination of the second sphere by the incident beam, the first particle must be quite large. So we consider for the first sphere a diameter of 225 nm, and a center-to-center distance 197.5 nm, but keep the same self-similar ratio as the previous nanolens design. We find a better more symmetric focusing conversion when the frequency is close to the Mie resonance of the middle particle. We plot such a case with excitation frequency of 625 nm in Fig. 8(a). The beam is transported through near-field coupling in the last particle, where we see a clear focus. Remarkably, there is almost no field along the beam's propagation direction after it encounters the self-similar array. Yet, the intensity of the focus compared to the intensity of the source seems to be lower in this design, as we see in Fig. 8(b). This can be attributed, to the field configuration of the excited Mie-plasmon on the first sphere. We witness strong but opposite in sign field areas which subsequently interact with the rest of the chain.

6. Conclusions

We studied optical excitations on metallic nano-sphere composites. We verified the applicability of the FDTD for the modeling of metallic nanoparticle based structures, within certain limitations. We investigated the intensity enhancement properties of silver nanosphere dimers and quadrumers. In particular we found dimers consisting of 100 nm in diameter spheres can lead to a high intensity enhancement factor comparable or exceeding enhancement factors emanating from smaller sized single spheres. This result is of particular interest considering the fact that larger particles are attainable by controlled techniques such as e-beam lithography [46]. We examined the conditions to control the polarization of the local enhanced field around the multimer, a pertinent feature for SERS applications [31]. We found a strong, subwavelength confinement of the enhanced field in the interstitial region of the dimers or quadrumers. The enhancement of such structures can be very broadband or more frequency selective. These characteristics could be utilized to make these type of dimers or quadrumers proper SNOM probes, thus surpassing the resolution barrier mandated by particle size [9, 47]. The reshaping of the field around the multimers could also make them relevant as building blocks in plasmon printing techniques [48]. Finally, we demonstrated two different nanolens designs which can convert a diffraction limited Gaussian beam into a subwavelength focus as small as one tenth the vacuum wavelength. In our longitudinal nanolens design we observed the formation of an isolated focus, thus in a functional location for the excitation of surface plasmon modes on related devices [40, 41, 42].

Acknowledgments

We would like to thank C. Oubre (Rice University) for fruitful discussions regarding the FDTD modeling of plasmonic nanostructures. In addition, we thank Prof. Ph. Lambin (LPS, FUNDP) for constructive comments in the course of this study. We also acknowledge Dr. R. Fikri (LPS, FUNDP), for useful discussions related to Scanning-Near field-Optical-Microscopy (SNOM). The present study was carried out within the framework of the Inter-University Attraction Pole (IUAP P5/01) on "Quantum size effects in nanostructured materials" of the Belgian Office for Scientific, Technical, and Cultural Affairs. We acknowledge the use of the Interuniversity Namur Scientific Computing Facility (Namur-ISCF), a common project between the Belgian National Fund for Scientific Research (FNRS), SUN Microsystems, and the Facultés Universitaires Notre-Dame de la Paix (FUNDP). C. Vandenbem was supported as research fellow by the FNRS. This work has also been partly supported by the Europian Regional Development Fund (ERDF) and the Wallon Regional Government under the "PREMIO" (Intereg IIIa) project.

#75920 - $15.00 USD Received 9 October 2006; revised 19 February 2007; accepted 20 March 2007